



1 **Technical note: Efficient imaging of hydrological units below lakes and fjords with a floating, transient**
2 **electromagnetic system (FloaTEM)**

3

4 Pradip Kumar Maurya¹, Frederik Ersted Christensen¹, M. Andy Kass¹, Jesper B. Pedersen¹, Rasmus R. Frederiksen¹,
5 Nikolaj Foged¹, Anders Vest Christiansen¹, and Esben Auken^{1,2}

6 ¹Department of Geoscience, HydroGeophysics Group Aarhus University, C.F. Møllers Alle, 4, Aarhus C, Denmark

7 ²The Geological Survey of Denmark and Greenland (GEUS) Oester Voldgade 10 1350 Copenhagen K Denmark, formerly at 1.

8 Corresponds to: pradip.maurya@geo.au.dk

9 **Abstract**

10 Imagining geological layers beneath lakes, rivers, and shallow seawater provides detailed information critical for
11 hydrological modelling, geologic studies, contaminant mapping, and more. However, significant engineering and
12 interpretation challenges have limited the applications, preventing widespread adoption in aquatic environments. We have
13 developed a towed transient electromagnetic (tTEM) system to a new, easily configurable floating, transient
14 electromagnetic instrument (FloaTEM) capable of imaging the subsurface beneath both fresh and saltwater water bodies.
15 Based on the terrestrial tTEM instrument, the FloaTEM system utilizes a similar philosophy of a lightweight towed
16 transmitter with a trailing, offset receiver, pulled by a small boat. The FloaTEM system is tailored to the specific fresh or
17 saltwater application as necessary, allowing investigations down to 100 m in freshwater environments, and up to 20 m on
18 saline waters. Through synthetic analysis we show how the depth of investigation of the FloaTEM system greatly depends
19 on the resistivity and thickness of the water column. The system has been successfully deployed in Denmark for a variety
20 of hydrologic investigations, improving the ability to understand and model processes beneath water bodies. We present
21 two freshwater applications and a saltwater application. Imaging results reveal significant heterogeneities in the sediment
22 types below the freshwater lakes. The saline water example demonstrates that the system is capable to identify and
23 distinguish clay and sand layers below the saline water column.

24 **1. Introduction**

25 Understanding interactions between surface water and groundwater is necessary for effective management of water
26 resources as they are both part of an interconnected hydrologic system (Sophocleous, 2002; Winter et al., 1998; Harvey
27 and Gooseff, 2015). This requires knowledge of hydrogeological settings below the water column of lakes, streams, and
28 other water bodies, in addition to properties underlying adjacent onshore areas. Non-invasive geophysical methods
29 provide spatial information on these subsurface properties and processes across many environments; over the last few
30 decades the methods have played a vital role in near-surface investigations (Barker, 1980; Hatch et al., 2010a; Day-Lewis
31 et al., 2006). However, deployment of surface-based geophysical investigations (as opposed to airborne systems) on
32 water bodies has historically been difficult (Sheets and Dumouchelle, 2009; Briggs et al., 2019; Parsekian et al., 2015);
33 while not insurmountable, this has limited the application range to some degree.

34 Electrical and electromagnetic methods (EM) are the two most-extensively used geophysical exploration and
35 characterization techniques for hydrologic applications (Binley and Kemna, 2005; Danielsen et al., 2003; Christiansen et



36 al., 2006; Auken et al., 2003; Minsley et al., 2021; Siemon et al., 2009). While classically used on land, several studies
37 have shown that these methods can also be used on lakes, streams, or rivers. Among the electrical methods, electrical
38 resistivity tomography (ERT) has been a common and robust technique, with applications to aquatic environments
39 including mapping the distribution of clay sediments, mapping freshwater saturation in saltwater bay sediments (Manheim
40 et al., 2004), and estimating sediment thicknesses and locating faults (Kwon et al., 2005). These studies deployed
41 relatively long floating cable layouts, or streamers, of approximately 100 meters, towed by a boat for collecting continuous
42 resistivity data. Longer cable layouts, giving deeper information, limit the operational efficiency significantly. This
43 implies that these instruments inherently have a limited depth of investigation (DOI).

44 Applications of transient electromagnetic (TEM) and frequency domain EM tools are reported in previous studies, e.g.,
45 discharge of groundwater to lakes and brines (Ong et al., 2010; Briggs et al., 2019), and extraction of lithium from large
46 scale natural brine systems (Munk et al., 2016). Airborne techniques have proved capable of mapping beneath lakes,
47 rivers and near-shore seas (Fitterman and Deszcz-Pan, 1998; Dickey, 2018; Rey et al., 2019), but are costly and provide
48 lower vertical and lateral resolution than their ground-based counterparts (Hatch et al., 2010b).

49 There has been a growing interest in the development of a towed, waterborne EM system, as such an instrument provides
50 continuous information with high lateral resolution. Mollidor et al. (2013) have shown an application of a commercial
51 in-loop transient EM (TEM) system on a volcanic lake to map sediment thickness. Since the system had a large transmitter
52 loop (18x18 m²), they encountered non 1D-effects requiring 3D modelling for proper interpretation. Hatch et al. (2010b)
53 presented results from a waterborne survey where they used a floating setup of a commercial TEM system, used over a
54 40 km section of the Murray River (Australia) to monitor the influx of saline water. These studies and systems, while
55 effective, have limitations preventing their widespread use in waterborne applications, specifically in terms of limited
56 DOI and horizontal resolution. An ideal system would be compact and lightweight, have a small footprint, and provide
57 sufficient transmitter power to investigate the hydrogeological properties beneath the water column.

58 Recent advancements in electronics of EM instrumentation led Auken et al. (2018) to develop a ground-based towed
59 transient electromagnetic system (tTEM) for efficient and high resolution 3D mapping of the subsurface (Maurya et al.,
60 2020). The tTEM system provides the necessary framework for creating a floating, towed EM system. The tTEM-system
61 is relatively compact, with the entire system extending no more than 16 m behind the towing vehicle and a maximum
62 width of 4 m. It has high lateral resolution, down to 10 m x 10 m. The tTEM also has a relative high transmitter moment
63 for such a compact system, providing depths of investigation in ground-based surveys down to 100m. The waterborne
64 version of the tTEM system is referred to as FloaTEM (see Fig.1) and a recent application of the FloaTEM system has
65 been presented by Lane et al. (2020) where they successfully used the ground configuration of the system on rivers and
66 estuaries in the United States to characterize the underlying hydrological system. In their study the system was used as it
67 was designed for ground-based applications (Auken et al., 2018) without any modifications to actual geometry and
68 measurements protocols. In this paper, we present a greatly improved and a flexible version of the FloaTEM system to
69 investigate subsurface properties beneath both fresh and saline water columns. We highlight the design aspects of the
70 system and discuss capabilities and limitations. Finally, we present three case studies to demonstrate the efficacy of the
71 FloaTEM system and interpretation methodology: surveying on a shallow freshwater lake, a deep freshwater lake, and in
72 a saline bay environment.



73 **2. The FloaTEM system**

74 Operating in aquatic environments provides challenges that are unique to the setting, requiring modifications not only to
75 the instrumentation relative to land-based operation, but also to acquisition protocols and safety procedures. Navigating
76 on shallow water, lakes, or rivers, may be challenging; to assist safe navigation, real time GPS and echo-sounder data are
77 integrated into the FloaTEM system's recording and navigation software. The echo-sounder provides the depth to the
78 river/lakebed and this information can furthermore be utilized as prior information in later data processing.

79 Design aspects of the FloaTEM system depends on the application—primarily whether freshwater or saltwater—and thus
80 we have designed both a fresh water FloaTEM system (FW-FloaTEM) and a saltwater FloaTEM system (SW-FloaTEM).
81 In the following, we discuss the details of freshwater and saltwater FloaTEM systems.

82 **2.1 The freshwater FloaTEM system**

83 The FW-FloaTEM has a design similar to the tTEM-system: A 4 x 2 m², single-turn transmitter coil (TX-coil) is followed
84 by the receiver coil (RX-coil), in a 9 m offset configuration. Figure 1 shows a schematic layout and photo of the FW-
85 FloaTEM system. The receiver coil has an effective area of 20 m² with a bandwidth of 420 kHz. This effective RX-area
86 is 4 times higher compared to the previously used RX-coil of the tTEM-system as described in Auken et al. (2018), and
87 therefore provides approximately a 4 times better signal to noise ratio and increased DOI (100m).

88 The fiberglass frame follows the same construction as the tTEM-system—mounted on two paddleboards instead of
89 sleds—and with additional frame components added for stability. The RX-coil is simply mounted on an inflatable rubber
90 boat. Note that all mounting and floatation devices of the TX- and RX-coils are of non-conductive materials to avoid EM
91 bias signals in the data.

92 The acquisition protocol consists of an alternating high- and low-moment transmitter pulse to obtain the sounding curve.
93 The low moment, with a peak current of ~3 A, records 15 time gates of data between 4 μs and 33 μs referenced to the
94 beginning of the turn-off of the transmitter pulse. The high-moment pulse utilizes 23 gates from 10 μs to 900 μs with a
95 peak current of ~30 A. Thanks to the latest hardware modification, the peak current is maintained with a deviation of
96 ±0.1A, which ensures a stable current waveform throughout the operation. Detailed system parameters are listed in Table-
97 1.

98 **2.2 The saltwater FloaTEM system**

99 Presence of highly conductive saltwater limits the DOI due to the slow diffusion of the eddy currents in the conductive
100 water body. In order to increase the DOI, the transmitter moment of the SW-FloaTEM is increased by a factor of eight,
101 compared to FW-FloaTEM, by doubling the transmitter loop size and increasing the number of TX-coil turns to four. The
102 saltwater configuration only utilizes a HM pulse of 25 A which is sufficient to obtain similar near surface resolution as
103 the freshwater system since the long-duration eddy currents in conductive seawater obviate the need to record very early
104 times. Further justification for using only HM is given in the synthetic studies section. Table-1 shows the parameters for
105 FW- and SW-FloaTEM systems. Observe that the last measurement gate for SW-FloaTEM is ~3 ms compared to ~1 ms
106 for FW-FloaTEM system.

107 The signal to noise ratio (S/N) is further increased by using a 40m² RX coil. As the limiting factor for these RX coils is
108 the noise in the pre-amplifier (Nyboe and Sørensen, 2012) increasing the area of the coil increases the S/N ratio



109 proportionally. This is true as long as the area is below approximately 200 m². Hence, the total S/N ratio increase for the
110 SW-FloaTEM system compared to the FW-FloaTEM system is a factor of 8 for the peak moment and a factor of two for
111 the RX- coil, in total a factor of 16.

112

113 **3. Model resolution study**

114 A model resolution study was conducted to investigate the influence of water depth and water conductivity on the
115 resolving capabilities of FloaTEM systems for the sub-water layers. The focus of the resolution study was the case of a
116 saltwater environment, where the conductive water layer limits the DOI significantly, and decreases the resolution of sub-
117 water resistivity structures. The model resolution study was also used in the design of the SW-FloaTEM system, and the
118 presented results therefore include both the FW- and SW-FloaTEM cases. The model resolution study comprises a) an
119 inversion of synthetically generated data from known layered models (the *true model*); b) a model parameter analysis of
120 the true models, and c) an estimated depth of investigation (DOI). The modelling was performed with a 1D framework,
121 and hence does not examine lateral resolution capabilities or ability to resolve 2D or 3D structures.

122 The modelling scheme consists of the following steps:

- 123 1. Calculate system-specific 1D forward data of the true model.
- 124 2. Estimate realistic data uncertainties on the forward data based on signal levels and background noise assumptions
- 125 3. Estimating model parameter uncertainties by a computation of the model covariance matrix for the true model.
126 (Auken et al., 2015)
- 127 4. Performing 1D smooth inversions of the forward data including DOI estimates.

128 All the modellings were carried out with the AarhusInv modelling code (Auken et al., 2015). The FW- and SW-FloaTEM
129 systems were modelled as described in Table 1. The data uncertainty was model dependent, based on a background noise
130 level at 1nV/m² at 1 ms plus a uniform contribution of 3%. The uniform uncertainty is the main contribution to data
131 uncertainty due to the relatively conductive models producing high signals. For the model parameter analysis, a priori
132 constraints on the water column were applied with a 10% uncertainty for the water depth and a 30% uncertainty for the
133 resistivity of the water. For the inversion, no lateral constraints were applied. However, for the model parameter analysis
134 lateral constraints were assumed between 5 similar neighboring models (based on the true model) to simulate the improved
135 resolution capabilities from information sharing when working with field data. For the inversion of the forward data, a
136 smooth 30-layer model description was used with logarithmic increasing layer thicknesses with depth, and with an
137 additional top layer representing the depth and resistivity of the water column. All inversions were carried out using a
138 homogenous starting resistivity model.

139 Two model sweeps were constructed, each consisting of 15 three-layer models (True models). In model sweep 1 (Fig.
140 2a), the thickness (water depth) was varied of a 0.3 Ωm top layer from one to 15 m. In model sweep 2 (Fig. 3a) the
141 resistivity of a 7 m thick water layer was varied from 0.1 - 3 Ωm. In both model sweeps, the second layer was 3 Ωm / 10
142 m thick, and the third layer 30 Ωm.



143 The modeling results for model sweep 1 are shown in Fig. 2. Since the modeling was carried out in log-model space, the
144 model parameter analysis (Fig. 2b and 2c) shows the relative uncertainties estimates (STD-factor) of the model
145 parameters. In general, a model parameter (resistivity or thickness) will be considered resolved if the STD-factor is less
146 than 1.5, moderately resolved if between 1.5-2.0 and unresolved if greater than 2. From the model parameter analysis in
147 Fig. 2b and 2c, we observe, as expected, that the resolution of the model in general decreases with increasing water depth.
148 The water layer is very well resolved in all cases partly because of the prior constraints and partly due to the method's
149 high sensitivity to the conductive water layer. In the SW-FloaTEM case (Fig. 2b) the resistivity of the second layer is
150 resolved (STD-factor < 2) to a water depth of about 7 m and the layer boundary between layer two and three (DEP 2) is
151 resolved to a water depth of about 10 m. In the FW-FloaTEM case the (Fig. 2c) the resistivity of the second layer is
152 resolved (STD-factor < 2) to a water depth of about 5 m and the layer boundary to a water depth of only around 4 m.
153 Also, for the third layer, the resistivity was better resolved in the SW-FloaTEM system case than in the FW case.

154 The inversion results of the true model data, with DOI estimates in Fig. 2d and 2e, are in-line with the observations from
155 the model parameter analysis. Increasing water depth results in a shallower DOI and loss of resolution of the sub-water
156 layers, and the SW-FloaTEM system performs better than the FW-FloaTEM system.

157 Water depth is not the only parameter of importance for the resolution capabilities, but also the resistivity or conductivity
158 of the water. Figure 3 shows the modeling results for model sweep 2 with a varying resistivity of a 7 m thick water layer.
159 For a very conductive water layer of 0.1-0.2 Ωm , the resolution is limited for both systems, as observed in the model
160 parameter analysis as well as in the inversion sections of Fig. 3. When the water resistivity is above 0.3-0.4 Ωm , the SW
161 system resolves/recovers the sub-water layers very well (Fig. 3b and 3d). Especially in resolving the boundary between
162 second and third layer (DEP2), the SW-system performs much better than the FW-system, which is also clearly reflected
163 in the DOI of the two systems.

164 Based on the presented analysis and other analyses (not shown in this paper), we conclude that the conductance (product
165 of conductivity and thickness) of the water column should be below approximately 25 Siemens for this particular SW-
166 FloaTEM system to be able to penetrate the water column and map sub-water layers. It was also clear that the S/N ratio for
167 the SW system had to be increased significantly compared to the FW system, but the very early time gates were not
168 needed, and a slower turn-off and lower bandwidth of the RX-coil was acceptable. This led to the compromise of more
169 turns in the transmitter coil, only high moment cycles and the larger area of the RX-coil.

170 4. Field cases

171 We present three surveys conducted with the FloaTEM system in Denmark: Two on freshwater lakes, and one on seawater
172 in a fjord. These datasets represent different water conductivities and various glacial sediment settings. Details of
173 processing and inversion of FloaTEM data are given in appendix-A. Some of the cases needed special handling of the
174 inversion process and this is described in the respective case study section. Table 2 summarizes key survey conditions
175 and modeling parameters.

176 4.1 Freshwater cases

177 We present two freshwater cases from two lakes in central Jutland, Denmark, to demonstrate the utility of the FloaTEM-
178 FW system in a shallow and a deep lake scenario.



179 **4.1.1 Lake Sunds**

180 Lake Sunds spans 127 hectares and is quite shallow (1.5 m - 2.5 m) with a maximum depth of 4.5 m. It is sitting in a late
181 Weichselian meltwater plain. The City of Sunds has developed around the lake, and the majority of the ~4000 inhabitants
182 of Sunds live close to the water. In recent years the groundwater table in Sunds has risen substantially, which causes
183 problems in the winter period where the groundwater is the highest and periods of heavy rain then results in flooded
184 cellars in residential houses. The problem is exacerbated by an old sewage system in the city with many worn pipes. These
185 pipes are under replacement, but this will remove the current drainage by worn pipes, and the consequences would be a
186 further rise of the groundwater table. On top of the flooding of cellars, there is a risk that the groundwater fluctuations
187 can mobilize near-surface pollutants from otherwise hydrologically inactive point-source pollutions in the city such as
188 old gas stations and landfills and hence contaminate the groundwater in the area.

189 From a hydrogeological viewpoint the shallow water table has puzzled the water managers as shallow boreholes from the
190 area show that the geology in the upper 20 meters is pure sand as expected in a meltwater plain environment. It was
191 therefore decided to setup a detailed groundwater model to investigate groundwater flow paths and identify measures to
192 control the groundwater table fluctuations.

193 The area to the east of the lake has been mapped with tTEM, covering a total of 816 hectares, with a FloaTEM survey
194 subsequently performed on the lake (Fig. 4). Additionally, multiple boreholes provide lithological data for comparison,
195 although the majority of the boreholes only reach 10-20 meters depth. Most of them were drilled in the 1940's in
196 connection to brown-coal mapping.

197 The tTEM and FloaTEM data were inverted separately, with the results combined in Figure 5. Profile A in Fig. 4 is
198 entirely on the lake and profile B is oriented north-south crossing the lake. In profile A, FloaTEM inversion results
199 generally show a good agreement with the available borehole description (B1 and B2) which is broadly categorized as
200 sand, clay and silt containing organic material. However, there is a slight mismatch between lithological boundaries
201 observed in some boreholes and inversion models. This mismatch may be caused by borehole offset from FloaTEM
202 profiles, possibly exaggerated by erroneous location data for the more than 70 years old logs. The distance of Borehole
203 B1 and B2 from the profile are 20 and 25m. Overall, the resistivity model indicates a presence of two areas with a thick
204 organic silt layer below the water column (Fig. 5a and 5c) followed by a thick and more resistive sand layer. The sand
205 layer thins out towards the bank of the lake and appears to go to the surface outside the lake as indicated in profile B. The
206 information about thickness and location of the organic silts are of great importance in the groundwater model of the area,
207 since these old lake deposits are impermeable and thereby guide groundwater flow beneath the lake.

208 Figure 5c-f shows mean resistivity maps at four depth intervals and includes both the FloaTEM and the tTEM survey
209 results. The mean resistivity maps indicate that there is a large degree of spatial variability of sediment types in and around
210 Lake Sunds. The heterogeneity beneath the lake would not be possible to resolve by interpolating across; this
211 heterogeneity is related to the lake genesis and reveals where the water table beneath the town of Sunds is in hydrologic
212 contact with the lake. Furthermore, the tTEM and FloaTEM results show that the geological setting is not a simple
213 sandbox at depth. At 20 meters depth and below we have several Tertiary clay layers with a resistivity of 10-30 ohm-m,
214 which have been deformed by glaciers and glacial tectonics. The information about the clay layers is crucial for the deeper
215 parts of the groundwater model.



216 **4.1.2 Lake Ravn**

217 Lake Ravn is located in Eastern Jutland, Denmark. It is the second deepest lake in Denmark with depths generally ranging
218 from 25 to 30 m, and with a maximum depth of 34 m. The lake was formed as a dead-ice hole located on top of a WSW-
219 ENE oriented partly-buried valley (Sandersen, 2016).

220 In the rOpen project (<https://hgg.au.dk/projects/ropen>), the Javngyde watershed northwest of Lake Ravn was mapped in
221 detail with tTEM, and it was modelled with a 3D finite difference groundwater flow model. The purpose of the rOpen
222 project was to estimate the total amount of nitrate reduction along flow pathways from the water table to a surface water
223 recipient. The rOpen work and a related hydrological modelling study (Rumph Frederiksen and Molina-Navarro, 2021)
224 revealed that around 40% of the infiltrating water crossed the surface watershed as groundwater flow to Lake Ravn.
225 However, the hydraulic connectivity between the watershed and the lake was poorly understood, and it was decided to
226 perform a FloaTEM survey on the lake to obtain more information about the hydrological system.

227 The survey was conducted with east/west oriented lines with a spacing of 60 m combined with lines encompassing the
228 perimeter of the lake (Fig. 6). Only electric boat engines are allowed on the lake, limiting the acquisition speed to 6 km/h.
229 Strong winds on the day of acquisition further challenged the navigation and resulting in head-wind lines being wigglier
230 than the tail-wind lines.

231 The resistivity model for Lake Ravn (Figure 7) shows multiple features of interest. The relatively high resistivity of the
232 lake water has allowed for extended depths of investigation, despite the deep-water column. The resistivity models have
233 a DOI down to 90 m below the lake surface. Within the water column we see resistivity changes, and this is verified by
234 direct current resistivity measurements conducted in 0.5 m depth intervals at multiple locations (not shown). The water
235 resistivity measurements were conducted using a 10 cm Wenner configuration. The measured resistivity of the water
236 column gradually varies from the top to the bottom of the lake, from ~27 to ~34 Ωm probably due to temperature
237 variations. For this reason, the water column was modeled with two resistivity layers with a priori constrained resistivity
238 values and a constrained water depth (depth to bottom of 2nd water layer), but with a free interface between the two water
239 layers. Beneath the bottom of the lake (Profile AA' and BB' in Fig. 6), we observe sandy layers, underlain by a clay layer
240 interpreted to be Oligocene. The mean resistivity maps (Fig. 7c-f) at different depths reveal a large heterogeneity in the
241 geology below Lake Ravn. Along the shore of the lake, we observe sandy deposits, which most likely play an important
242 role in discharging groundwater to the lake.

243 **4.2 Saltwater study**

244 Horsens bay is a shallow fjord located in the western Baltic sea, Denmark, roughly 18 km long and 2-3 km wide. It has
245 poor ecological status, possibly due to submarine groundwater discharge causing excessive loading of nutrients (Hinsby
246 et al., 2012). Increased loading of nutrients has caused the Baltic sea as one of the most polluted seas in the world
247 (Pihlainen et al., 2020; Meier et al., 2019). To understand the vulnerability of the Horsens Fjord and coastal zone dynamics
248 an improved understanding of land-sea interactions including contaminant pathways in the subsurface, in relation to
249 nutrient and salinity variations, is needed.

250 The water depth within the survey area (Fig. 8) ranges from 2 m (minimum water depth for safe maneuverability with the
251 specific vessel) to 8 m in the central area. FloaTEM data were acquired in North-South striking lines across the bay



252 (Figure 8), with a line spacing of ~25 m and an operational speed of 12-14 km/h. The relatively small survey was
253 conducted in collaboration with the Geological Survey of Denmark and Greenland (GEUS). The purpose was to identify
254 and map fresh groundwater flow into the fjord, which may provide pathways for nitrate leaching from the surrounding
255 farmland into the bay. The geology beneath the Horsens fjord includes quaternary meltwater sand and gravel constituting
256 as aquifer and quaternary clay tills and Miocene mica clay as aquitards (Jørgensen et al., 2010). A narrow channel connects
257 the fjord to deeper waters in the Baltic Sea. The central part of the fjord is dominated by muddy sediments due to the high
258 accumulation of organic material. Till deposits are present in shallow coastal areas.

259 FloaTEM inversion results are presented in Fig. 9. The resistivity model in Horsens Bay (profile A in Figure 9) constitutes
260 a three-layer model where the top layer is the sea water followed by a conductive clay-rich infill sediments, likely an
261 extension of the Tørring/Horsens valley (Sandersen, 2016). The sequence is generally fining-upward, with significant
262 imprints of paleo-topography. Below the clay-rich layer, a third layer with elevated resistivity is present; interpreted as a
263 meltwater sand unit but saturated with sea water. The resistivity of this sand unit appears to be low (10-15 ohm-m)
264 compared to one would expect for fresh water saturated sand. This sandy unit is most likely leading the groundwater
265 discharge into the seabed at locations where the overlaying clay-till unit is sufficiently thin.

266 The mean resistivity maps (Fig. 9 b-e) show the spatial variability of the clay-till and sand rich sediments at four depth
267 intervals below the sea water label. We see that the sediment close to the coast has a higher resistivity than what is
268 observed in the middle of the fjord. This might be a transition from a sandy sediment towards a more clay-rich
269 environment in the middle of the fjord. The knowledge of extension of these sand rich sediments from coast to the middle
270 of fjord, helps us to locate the probable regions where groundwater may discharge into fjord. Additionally, we also
271 observe a small, northwest trending low resistivity structure indicates a paleo-channel, which has been confirmed by
272 shallow-seismic data (not shown).

273 5. Discussion

274 The resistivity of a surface water body can change over short distances, so inversions will often benefit from a spatially
275 varying resistivity constraint or reference. The need for a priori water resistivity and depth is higher in the freshwater
276 cases than the saltwater case. The high conductivity in saltwater environments usually results in a well-resolved water
277 column, so a priori information is less important. While the current instrument is integrated with a depth sounder, it is not
278 difficult to fit it with a conductivity logger as well to supply relevant a priori values for the water column. We note that
279 the choice in towing vessel is important as a larger vessel requires a longer towing distance.

280 In general, the data quality for FloaTEM is usually better than comparable land surveys as lakes and rivers are often far
281 from interfering infrastructure, which means that a FloaTEM survey normally results in full data coverage without gaps
282 from data culling.

283 FloaTEM data provide critical information regarding sub-lake or sub-sea geology. In the Lake Sunds example, an
284 interpretation based on land data only with lithological boundaries interpolated across the lake would be quite erroneous
285 by missing the unique features associated with the genesis of the lake. The FloaTEM system provides a means of capturing
286 these features which would be infeasible to identify with boreholes.



287 The depth of investigation is highly dependent on not only the resistivities of soils, but also of the conductivity of the
288 waters as the synthetic modeling study showed, where even a small conductivity change in the saltwater can reduce the
289 DOI significantly. This stresses that a priori information about water salinity values is critical in selecting between the
290 FW-FloaTEM and SW-FloaTEM configurations and designing the particular survey design.

291 The high signal level in conductive saltwater environments often results in very low noise, also at the latest recorded time
292 gate at ~2 ms. In these cases, increasing the recording time and reducing the repetition rate should increase the DOI by
293 adding more late-time data. However, a lower repetition rate may also lead to higher motion induced noise in the receiver
294 coil, which can become the dominating noise for the late time gates.

295 The results showed here all focused on delineation of hydrological permeable (sands) and impermeable (clays) lithologies
296 in the context of improving large-scale hydrological understanding and prediction strength. Though, from the given
297 examples it should be clear that the application range of FloaTEM spans much more. A few examples include foundation
298 investigations for offshore wind farms; raw material exploration beneath lakes and rivers; and geotechnical pre-
299 investigations for cabling routes below water bodies.

300 **6. Conclusions**

301 We have developed a new towed, easily configurable floating TEM instrument, FloaTEM, and successfully applied the
302 system to both freshwater and saltwater studies to investigate geology and hydrology beneath lakes and shallow seawater.
303 The FloaTEM system is modular, so longer beams can be used to increase the transmitter moment and likewise more
304 transmitter turns can be added, both increasing the depth of investigation. Supported by synthetic analysis, we
305 reconfigured a freshwater FloaTEM system to a saltwater FloaTEM system, primarily by increasing the transmitter
306 moment and decreasing the noise in the receiver coil enabling us to perform FloaTEM surveys not only on both shallow
307 and deep lakes, but also on shallow saltwater up to 8 meters deep.

308 The conductance of the water, water depth multiplied with water conductivity, is the limiting factor when surveying on
309 saline water. Based on the presented analysis the water column should be below ~25 Siemens for the system to penetrate
310 the water column and map sub-water layers. For freshwater lakes and rivers, depths of investigation of 80 meters or more
311 are possible, while in saltwater cases we can achieve depths of investigation of 10-25 meters strongly depending on water
312 depth and conductivity.

313 With the FloaTEM system, we can map geological layers beneath the water bodies, normally not accessible for mapping
314 with ground based geophysical methods, thereby allowing for detailed hydrological modelling in these often-important
315 areas as well. Through 2 freshwater cases and one saltwater case we show the system's ability to image the heterogeneous
316 geology beneath water bodies. In the freshwater cases the FloaTEM datasets revealed geological information that would
317 have been impossible to deduce from land-based-only information and in the saltwater case the data delivered clear images
318 on the clay-sand distribution beneath the seafloor.

319 **7. Author contribution**

320 PM design and develop methodology, instrumentation, data processing and inversion, wrote the first draft of manuscript.
321 FC carried out data collection, data analyses and contributed to original manuscript. JP and MK contributed to first draft
322 of the manuscript and interpretations and feedback on inversion results. RF provided data interpretations, feedback and



323 contributed to the writing of original manuscript. NF carried out synthetic data analysis and field data inversion of Ravnø
324 lake. AV and EA conceptualized the methodology, contributed to writing original manuscript and provided feedback.

325 **8. Acknowledgements**

326 We thank TOPSOIL, an Interreg project supported by the North Sea Programme of the European Regional Development
327 Fund of the European Union, and the development has been funded by Innovation Fund Denmark, project rOpen (Open
328 landscape nitrate retention mapping) and MapField (Field-scale mapping for targeted N-regulation), WATEC (Aarhus
329 university Centre for water technology) and internal HGG (Hydrogeophysics group at Aarhus university) funding. Partial
330 support for data collection and interpretation of results were provided by GEUS (Geological survey of Denmark and
331 Greenland).

332 **References**

- 333 Auken, E., Jørgensen, F., and Sørensen, K. I.: Large-scale TEM investigation for groundwater, *Exploration*
334 *Geophysics*, 33, 188-194, 2003.
- 335 Auken, E., Christiansen, A. V., Westergaard, J. A., Kirkegaard, C., Foged, N., and Viezzoli, A.: An integrated
336 processing scheme for high-resolution airborne electromagnetic surveys, the SkyTEM system,
337 *Exploration Geophysics*, 40, 184-192, 2009.
- 338 Auken, E., Foged, N., Larsen, J., Lassen, K., Maurya, P., Dath, S., and Eiskjær, T.: tTEM — A towed transient
339 electromagnetic system for detailed 3D imaging of the top 70 m of the subsurface, *GEOPHYSICS*, E13-
340 E22, 10.1190/geo2018-0355.1, 2018.
- 341 Auken, E., Christiansen, A. V., Fiandaca, G., Schamper, C., Behroozmand, A. A., Binley, A., Nielsen, E., Effersø,
342 F., Christensen, N. B., Sørensen, K. I., Foged, N., and Vignoli, G.: An overview of a highly versatile
343 forward and stable inverse algorithm for airborne, ground-based and borehole electromagnetic and
344 electric data, *Exploration Geophysics*, 2015, 223-235, 2015.
- 345 Barker, R. D.: Applications of geophysics in groundwater investigations, *Water Services*, 84, 1980.
- 346 Binley, A. and Kemna, A.: DC Resistivity and Induced Polarization Methods, in: *Hydrogeophysics*, edited by:
347 Rubin, Y., and Hubbard, S. S., Springer Netherlands, Dordrecht, 129-156, 10.1007/1-4020-3102-5_5,
348 2005.
- 349 Briggs, M. A., Nelson, N., Gardner, P., Solomon, D. K., Terry, N., and Lane, J. W.: Wetland-Scale Mapping of
350 Preferential Fresh Groundwater Discharge to the Colorado River, 57, 737-748,
351 <https://doi.org/10.1111/gwat.12866>, 2019.
- 352 Christiansen, A. V., Auken, E., and Sørensen, K. I.: The transient electromagnetic method, in: *Groundwater*
353 *Geophysics. A tool for hydrogeology*, 1 ed., edited by: Kirsch, R., Springer, 179-224, 2006.
- 354 Danielsen, J. E., Auken, E., Jørgensen, F., Søndergaard, V., and Sørensen, K. I. J. o. a. g.: The application of
355 the transient electromagnetic method in hydrogeophysical surveys, 53, 181-198, 2003.
- 356 Day-Lewis, F. D., White, E. A., Johnson, C. D., Lane, J. W., and Belaval, M.: Continuous resistivity profiling to
357 delineate submarine groundwater discharge—examples and limitations, *The Leading Edge*, 25, 724-
358 728, 10.1190/1.2210056, 2006.
- 359 Dickey, K. A.: Geophysical investigation of the Yellowstone Hydrothermal System, *Geophysics*, Virginia Tech,
360 110 pp., 2018.
- 361 Fitterman, D. V. and Deszcz-Pan, M.: Helicopter EM mapping of saltwater intrusion in Everglades National
362 Park, Florida, *Exploration Geophysics*, 29, 240-243, 10.1071/EG998240, 1998.
- 363 Harvey, J. and Gooseff, M.: River corridor science: Hydrologic exchange and ecological consequences from
364 bedforms to basins, 51, 6893-6922, <https://doi.org/10.1002/2015WR017617>, 2015.
- 365 Hatch, M., Munday, T., and Heinson, G.: A comparative study of in-river geophysical techniques to define
366 variations in riverbed salt load and aid managing river salinization, 75, WA135-WA147,
367 10.1190/1.3475706, 2010a.



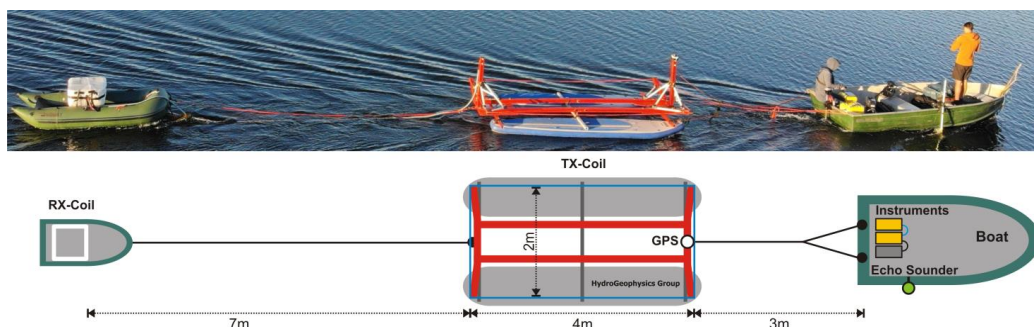
- 368 Hatch, M., Munday, T., and Heinson, G.: A comparative study of in-river geophysical techniques to define
369 variations in riverbed salt load and aid managing river salinization, *Geophysics*, 75, WA135-WA147,
370 2010b.
- 371 Hinsby, K., Markager, S., Kronvang, B., Windolf, J., Sonnenborg, T., and Thorling, L.: Threshold values and
372 management options for nutrients in a catchment of a temperate estuary with poor ecological status,
373 *Hydrology and Earth System Sciences*, 16, 2663-2683, 2012.
- 374 Jørgensen, F., Møller, R. R., Sandersen, P. B., and Nebel, L.: 3-D geological modelling of the Egebjerg area,
375 Denmark, based on hydrogeophysical data, *GEUS Bulletin*, 20, 27-30, 2010.
- 376 Kwon, H.-S., Kim, J.-H., Ahn, H.-Y., Yoon, J.-S., Kim, K.-S., Jung, C.-K., Lee, S.-B., and Uchida, T. J. E. G.:
377 Delineation of a fault zone beneath a riverbed by an electrical resistivity survey using a floating
378 streamer cable, 36, 50-58, 2005.
- 379 Lane, J. W., Briggs, M. A., Maurya, P. K., White, E. A., Pedersen, J. B., Auken, E., Terry, N., Minsley, B., Kress,
380 W., LeBlanc, D. R., Adams, R., and Johnson, C. D.: Characterizing the diverse hydrogeology underlying
381 rivers and estuaries using new floating transient electromagnetic methodology, *Science of The Total
382 Environment*, 740, 140074, <https://doi.org/10.1016/j.scitotenv.2020.140074>, 2020.
- 383 Manheim, F. T., Krantz, D. E., and Bratton, J. F.: Studying Ground Water Under Delmarva Coastal Bays Using
384 Electrical Resistivity, 42, 1052-1068, <https://doi.org/10.1111/j.1745-6584.2004.tb02643.x>, 2004.
- 385 Maurya, P. K., Christiansen, A. V., Pedersen, J. B., and Auken, E.: High resolution 3D subsurface mapping using
386 a towed transient electromagnetic system - tTEM: case studies, *Near Surface Geophysics*, 18, 16,
387 10.1002/nsg.12094, 2020.
- 388 Meier, H., Edman, M., Eilola, K., Placke, M., Neumann, T., Andersson, H. C., Brunnabend, S.-E., Dieterich, C.,
389 Frauen, C., and Friedland, R.: Assessment of uncertainties in scenario simulations of biogeochemical
390 cycles in the Baltic Sea, *Frontiers in Marine Science*, 6, 46, 2019.
- 391 Minsley, B. J., Rigby, J. R., James, S. R., Burton, B. L., Knierim, K. J., Pace, M. D. M., Bedrosian, P. A., and Kress,
392 W. H.: Airborne geophysical surveys of the lower Mississippi Valley demonstrate system-scale
393 mapping of subsurface architecture, *Communications Earth & Environment*, 2, 131, 10.1038/s43247-
394 021-00200-z, 2021.
- 395 Mollidor, L., Tezkan, B., Bergers, R., and Löhken, J.: Float-transient electromagnetic method: in-loop transient
396 electromagnetic measurements on Lake Holzmaar, Germany, *Geophysical Prospecting*, 61, 1056-
397 1064, 10.1111/1365-2478.12025, 2013.
- 398 Munk, L., Hynek, S., Bradley, D. C., Boutt, D., Labay, K. A., and Jochens, H.: Lithium brines: A global
399 perspective: Chapter 14, 2016.
- 400 Nyboe, N. S. and Sørensen, K. I.: Noise reduction in TEM: Presenting a bandwidth- and sensitivity-optimized
401 parallel recording setup and methods for adaptive synchronous detection, *Geophysics*, 77, E203-
402 E212, 2012.
- 403 Ong, J. B., Lane, J. W., Zlotnik, V. A., Halihan, T., and White, E. A.: Combined use of frequency-domain
404 electromagnetic and electrical resistivity surveys to delineate near-lake groundwater flow in the
405 semi-arid Nebraska Sand Hills, USA, *Hydrogeology Journal*, 18, 1539-1545, 10.1007/s10040-010-
406 0617-x, 2010.
- 407 Parsekian, A. D., Singha, K., Minsley, B. J., Holbrook, W. S., and Slater, L.: Multiscale geophysical imaging of
408 the critical zone, 53, 1-26, <https://doi.org/10.1002/2014RG000465>, 2015.
- 409 Pihlainen, S., Zandersen, M., Hyttiäinen, K., Andersen, H. E., Bartosova, A., Gustafsson, B., Jabloun, M.,
410 McCrackin, M., Meier, H. M., and Olesen, J. E.: Impacts of changing society and climate on nutrient
411 loading to the Baltic Sea, *Science of the Total Environment*, 731, 138935, 2020.
- 412 Rey, D. M., Walvoord, M. A., Minsley, B., Rover, J., and Singha, K.: Investigating lake-area dynamics across a
413 permafrost-thaw spectrum using airborne electromagnetic surveys and remote sensing time-series
414 data in Yukon Flats, Alaska, *Environmental Research Letters*, 14, 025001, 10.1088/1748-9326/aaf06f,
415 2019.



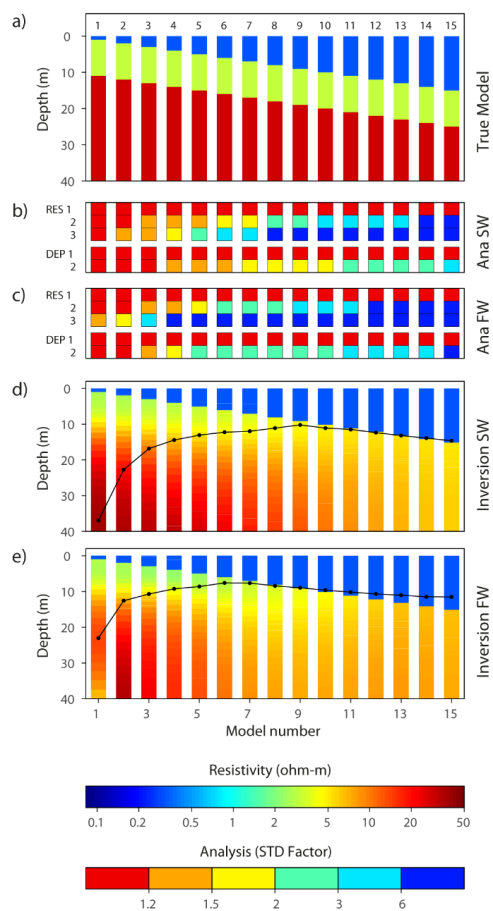
- 416 Rumph Frederiksen, R. and Molina-Navarro, E.: The importance of subsurface drainage on model
417 performance and water balance in an agricultural catchment using SWAT and SWAT-MODFLOW,
418 Agricultural Water Management, 255, 107058, <https://doi.org/10.1016/j.agwat.2021.107058>, 2021.
- 419 Sandersen, J. F.: Kortlægning af begravede dale i Danmark. Opdatering 2015. GEUS Særudgivelse.,
420 [http://begravededale.dk/PDF_2015/091116_Rapport_Begravede_dale_BIND_1_Endelig_udgave.p](http://begravededale.dk/PDF_2015/091116_Rapport_Begravede_dale_BIND_1_Endelig_udgave.pdf)
421 [df](http://begravededale.dk/PDF_2015/091116_Rapport_Begravede_dale_BIND_1_Endelig_udgave.pdf), 2016.
- 422 Sheets, R. and Dumouchelle, D.: Geophysical Investigation Along the Great Miami River From New Miami to
423 Charles M. Bolton Well Field, Cincinnati, Ohio, U. S. Geological Survey, 2009.
- 424 Siemon, B., Christiansen, A. V., and Auken, E.: A review of helicopter-borne electromagnetic methods for
425 groundwater exploration, Near Surface Geophysics, 7, 629-646, 2009.
- 426 Sophocleous, M.: Interactions between groundwater and surface water: the state of the science,
427 Hydrogeology journal, 10, 52-67, 2002.
- 428 Viezzoli, A., Auken, E., and Munday, T.: Spatially constrained inversion for quasi 3D modelling of airborne
429 electromagnetic data - an application for environmental assessment in the Lower Murray Region of
430 South Australia, Exploration Geophysics, 40, 173-183, 2009.
- 431 Winter, T. C., Harvey, J. W., Franke, O. L., and Alley, W. M.: Ground Water and Surface Water A Single
432 Resource 1139, 1998.

433 List of Figures

434

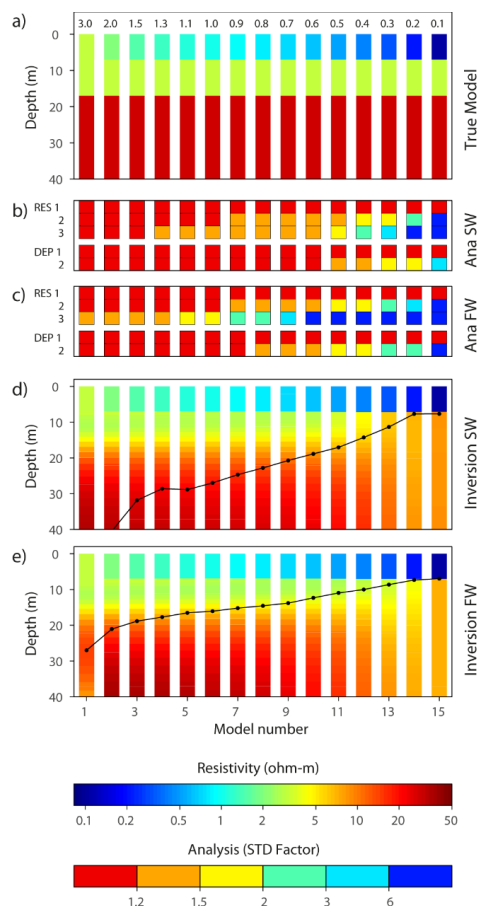


435 **Figure 1: Picture and schematic of the freshwater FloaTEM configuration, with boat, transmitter coil (TX-coil), and receiver**
436 **coil (RX-coil). In contrast, the saltwater configuration uses a 4m x 4m transmitter coil.**



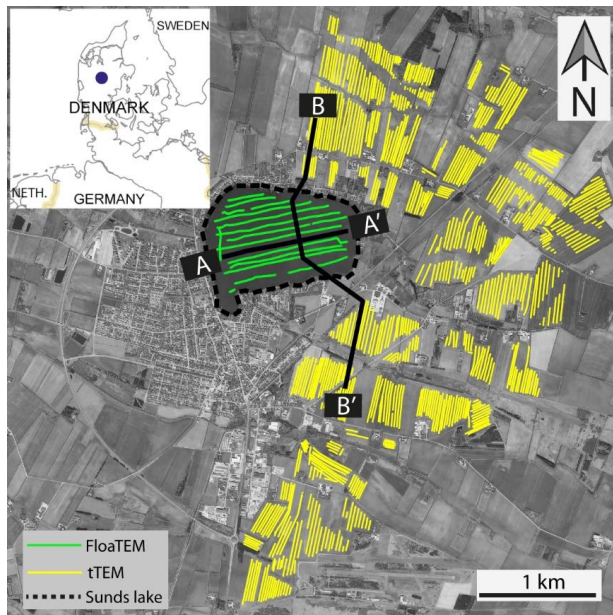
437

438 **Figure 2.** a) True model. Number on top of each model bar states the water depth (thickness of first layer). b-c) Model parameter
439 analyses of the true models, stated as a standard deviation factor, for the SW- and FW-FloaTEM systems. d-e) Inversion results
440 for SW- and FW-FloaTEM systems. The black line shows the DOI.



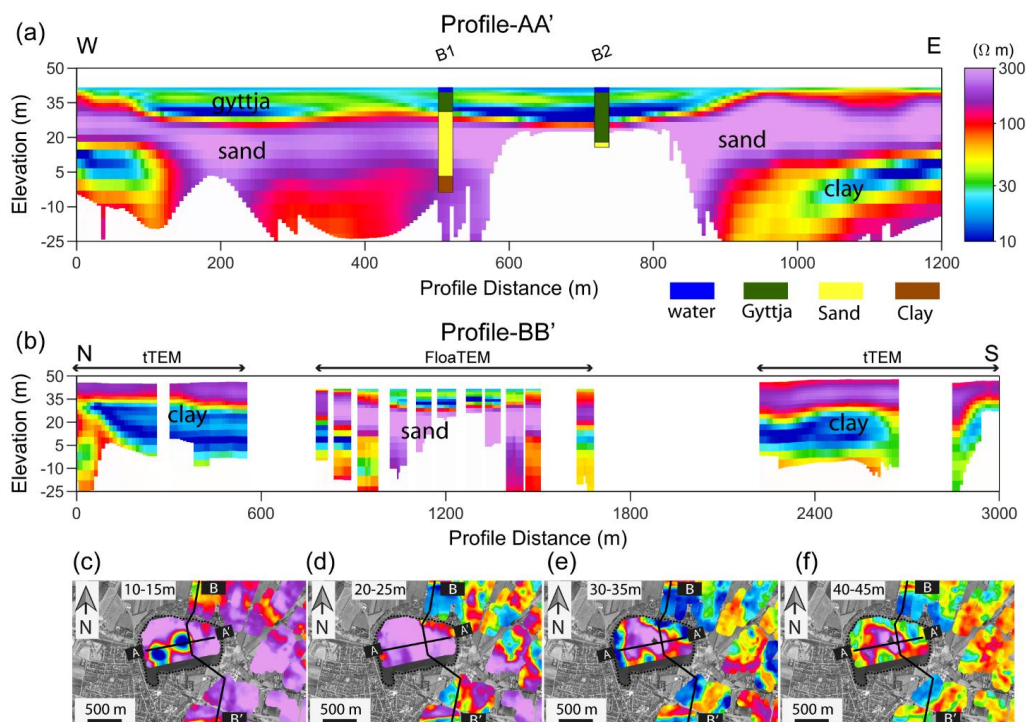
441

442 **Figure 3. Model sweep 2. a) True model. Number on top of each model bar states the resistivity of the water (resistivity of first**
 443 **layer). b-c) Model parameter analysis of the true model, stated as standard deviation factor, for the SW- and FW-FloaTEM**
 444 **systems. d-e) Inversion results for SW- and FW-FloaTEM systems. The black line shows the DOI.**



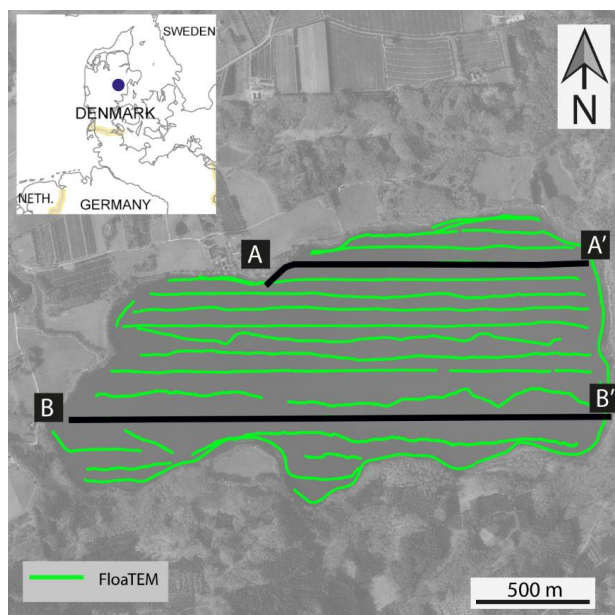
445

446 **Figure 4 Sunds FloaTEM and tTEM survey region with FloaTEM lines marked in green and tTEM in yellow. AA' and BB'**
447 **are the profiles that are presented in Figure 5.**



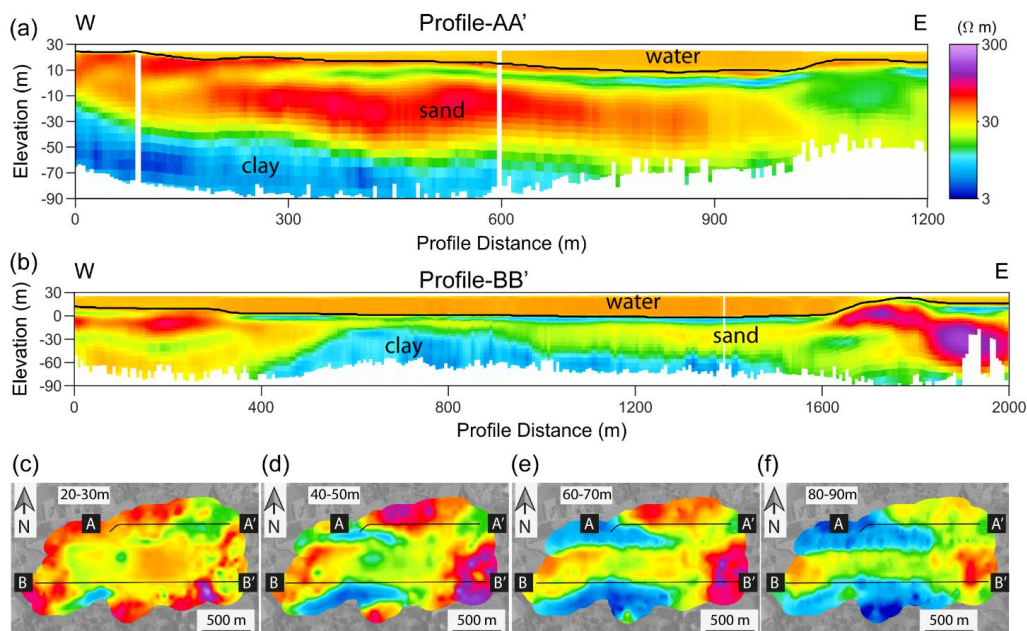
448

449 **Figure 5: Results from Sunds joint tTEM and FloaTEM survey. Location of profile AA' and BB' is marked in Error! Reference**
 450 **source not found.; note that while the elevation axis is identical, the profiles have different lengths and thereby different vertical**
 451 **exaggeration. Profile-AA' includes lithological interpretations from available boreholes near the survey line. Note that the**
 452 **water column is included in the figure, but only 2 meters thick, (c) - (f) show mean-resistivity maps at various depth intervals**
 453 **with profile -AA' and BB' indicated as solid black line. Lake Sunds is marked with dotted black line.**



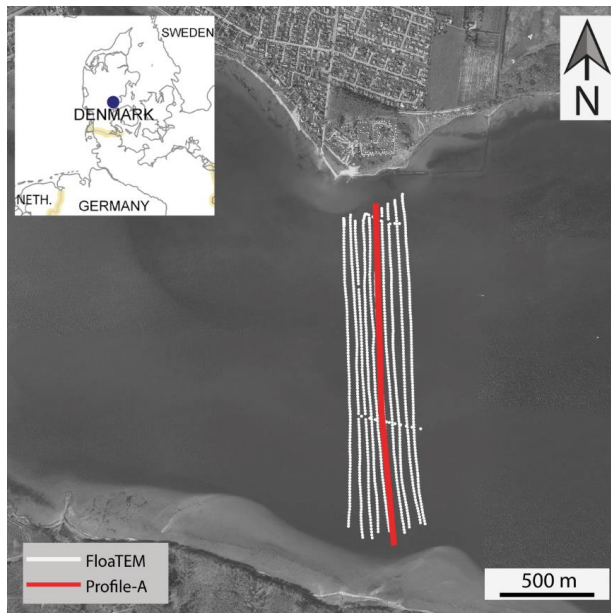
454

455 **Figure 6: Survey region for the Lake Ravn FloaTEM survey. Locations of the profiles in Figure 7 are highlighted as solid**
456 **black lines**



457

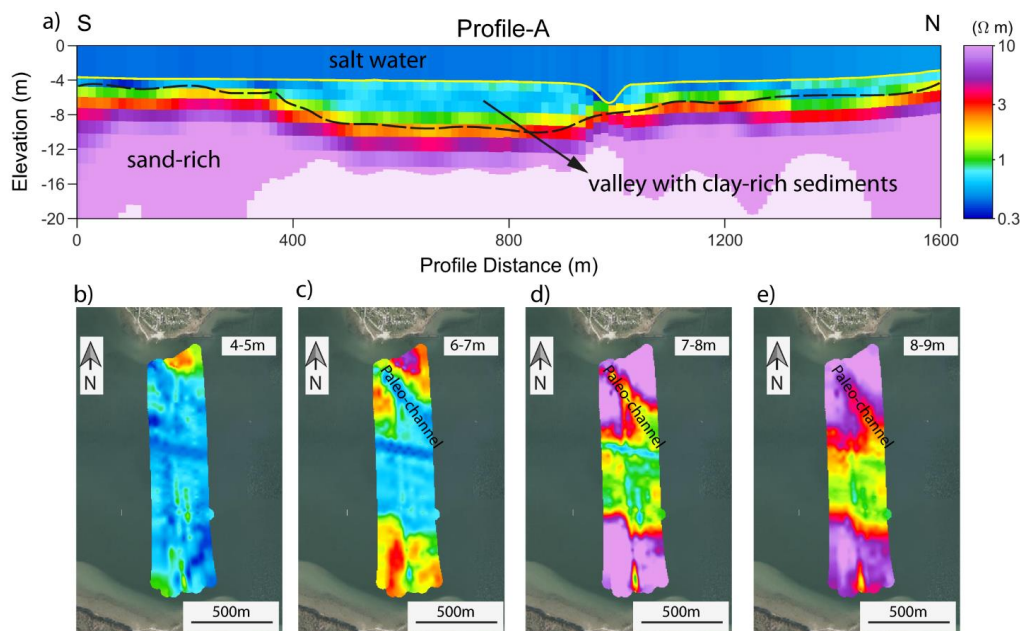
458 **Figure 7: Results from Lake Ravn FloaTEM survey. Location of the resistivity sections AA' and BB' are marked in Error!**
 459 **Reference source not found.. The black line in the sections marks the lake bottom while the white faded colors indicate the DOL.**
 460 **(c) – (f) show mean-resistivity maps at 4 depth intervals below surface together with location of profile AA' and BB'.**



461

462 **Figure 8: Horsens Bay with FloaTEM survey lines. The red highlighted profile marks the location of the resistivity section**
463 **showed in figure. 9**

464



465

466 **Figure 9: Resistivity mapping results from Horsens Bay. (A) Resistivity section (location marked in Figure 8) with**
 467 **the seafloor marked with the yellow line. (b-e) Mean resistivity maps at different depths.**

468 **List of Tables**

469

| FloaTEM system | FW-FloaTEM | | SW-FloaTEM |
|--|---------------------|----------------------|----------------------|
| | Low moment | High moment | High moment |
| Transmitter area | 8 m ² | | 16 m ² |
| Number of turns | 1 | | 4 |
| TX peak current | ~3 A | ~30 A | ~25 A |
| TX peak moment | ~24 Am ² | ~240 Am ² | 1600 Am ² |
| Repetition frequency @ 50 Hz power line frequency | 2110 Hz | 630 Hz | 220 Hz |
| Duty cycle | 42% | 30% | 22% |
| Tx on-time | 200 μs | 450 μs | 1000 μs |
| Turn-off time | 2.6 μs | 4.5 μs | 14.10 μs |
| Gate time interval (from beginning of turn-off) | 4-33 μs | 10-900 μs | 20-2800 μs |
| <i>RX coil area</i> | 20 m ² | 20 m ² | 40 m |
| <i>RX coil bandwidth</i> | 420 kHz | 420 kHz | 140 k Hz |
| Number of gates | 15 | 23 | 26 |

470

471

Table 1: System parameters for the freshwater and saltwater FloaTEM systems.

472



| Survey area | Max. water depth | System | Line spacing nominal | Water depth prior constraint | Water resistivity, prior constraint |
|---------------|------------------|------------|----------------------|------------------------------|---|
| Lake Sunds | 4.5 m | FW-FloaTEM | 50 m | 1.03 | 15 Ω m, None |
| Lake Ravn | 34 m | FW-FloaTEM | 60 m | 1.05 | *28 Ω m, 1.1 *34 Ω m, 1.05 |
| Horsens fjord | 8 m | SW-FloaTEM | 35 m | 1.05 | 0.3 Ω m, None |

473

474 **Table 2: Survey configurations and conditions of the three case areas. The * indicates that the water column was modeled with**
475 **two resistivity layers.**

476

477 **Appendix-A**

478 **Data processing and inversion**

479 In this section, we give an overview of the data processing and inversion scheme used for FloaTEM data. In each of the
480 case studies, FloaTEM data were processed with the Aarhus Workbench software from Aarhus GeoSoftware
481 (www.arhusgeosoftware.dk). The standard FloaTEM processing flow follows Auken et al. (2009). Raw db/dt data are
482 first processed to remove coherent coupling interference due to nearby infrastructures and then stacked to produce
483 soundings with approximately 10 m spacing. In the presented cases, a short smoothing filter was applied on the recorded
484 water depth data, but this step depends on the quality of the depth sounder data at hand. A preliminary inversion is then
485 performed to evaluate and adjust the first-step processing of raw db/dt data.

486 The final inversions of the FloaTEM data were carried out using a spatially constrained inversion formulation, SCI
487 (Viezzoli et al., 2009) using a 30 layer smooth model with layer thicknesses of layers 2-30 increasing logarithmically
488 down to 120 m. The thickness of layer 1 is set to the water depth with a fairly tight prior constraint. No vertical resistivity
489 constraints are applied from the water layer (layer 1) to the sub-layers (layers 2-30), hereby allowing a shape boundary at
490 the lake-/ seabed in the inversion results. The water depth prior information can be taken from the echo-sounder data or
491 from an external bathymetry grid. Additionally, prior constraints can be added to the resistivity of the water layer if
492 separate measurement of the water conductivity are present. In some cases, it is insufficient to model the water column
493 as one homogeneous layer, e.g. probably due to a halocline or thermocline. In these cases, more layers are introduced to
494 represent the water column in the inversion setup and the prior water depth is assigned to the depth to the bottom of the
495 last water layer.

496